Article

Digitally Chirped Multilayer Quantum Dot Lasers with Dual-Wavelength Lasing Emissions

Yi-Jan Leo Sun, Pin-Hsien Hsieh and Gray Lin * (ID)

Institute of Electronics, National Chiao Tung University, Hsinchu City 30010, Taiwan;
leoheatblast@gmail.com (Y.-J.L.S.); qqalan821@gmail.com (P.-H.H.)
* Correspondence: graylin@mail.nctu.edu.tw; Tel.: +886-3-513-1289

check for updates

Abstract: The dual-wavelength lasing emissions of digitally chirped multilayer quantum dot (QD) lasers are investigated both experimentally and theoretically. The two lasing wavelengths are both identified as ground-state (GS) emissions but originated from different stacks of QD multilayers. The lasing spectra exhibited broadening and splitting properties by injecting more current. Moreover, the wavelength-resolved light-current characteristics reveal that first GS lasing intensity upon the threshold of second GS transitions neither saturates nor droops with increasing injection current, but increases with slightly reduced slope efficiency. A theoretical model is developed for digitally chirped multilayer QD lasers. The simulation results qualitatively reproduce the experimental observations.

Keywords: quantum dots; semiconductor lasers; dual-wavelength lasers; rate equations

1. Introduction

Quantum dot (QD) heterostructures based on self-assembled growth are developed as ultimate control of free carriers over the nanometer scale in three dimensions. Semiconductor gain elements incorporating QD heterostructure have been emerging since the early 1990s [1]. The limited QD density and dispersed QD size render the optical gain characteristics quite different from quantum well (QW) heterostructure. At first, multiple QD layers were grown to prevent gain saturation in high modal gain devices of short cavity edge emitting lasers [2] and vertical cavity surface emitting lasers [3]. Then, Chirped QD multilayers were designed to achieve a wide emission spectrum in suplerluminecent diodes [4] and broadband laser diodes [5,6]. Afterwards, chirped QD multilayers found novel applications in external-cavity QD lasers, mode-locked QD lasers, and dual-wavelength QD lasers [7–10].

The emission spectral range and luminescent peak of InAs QDs are quite sensitive to growth parameters as well as matrix materials. Stacking of multiple QD layers with different InAs monolayers in QDs is not practical as dot density and radiative efficiency are subject to large variation. To reproducibly control the gain bandwidth of chirped QD multilayers, it is preferred to vary either thickness or In composition of InGaAs matrix surrounding InAs QDs [6]. In practice, the emission wavelength of individual InAs/InGaAs QD layer is continuously chirped (CC) in multilayer QD (MQD) stacks and referred to as CC-MQD in short. However, the parameter of multilayer is neither fully exploited in experiments nor ingeniously introduced in simulation. We have patented the digitally chirped multilayer QD stacks, referred to as DC-MQD, by designing a plurality of QD emission wavelengths, each of which is stacked with different QD layer numbers [7]. The conventional multilayer QD stacks with uniform emission wavelength for individual QD layer are referred to as Uni-MQD.

The features of DC-MQD gain media are in two folds. First, the chirped wavelengths are predetermined and clearly separated so that lasing wavelengths can be identified from different layers of QD stack. Second, the optical gain spectra can be engineered independently for individual wavelength through layer numbers. We have incorporated DC-MQD to develop novel devices of dual-wavelength QD edge emitting lasers with simultaneous two lasing wavelengths around threshold [8], low threshold current and widely tunable external cavity QD lasers [9], dual-wavelength and ground-state (GS) mode-locked QD lasers with a wide operation range [10].

In this paper, QD edge emitters with dual-wavelength lasing emissions are revisited. The slope efficiency for individual lasing wavelength is investigated both experimentally and theoretically. This paper is organized as follows. Section 2 presented the wavelength-resolved light-current (L-I) characteristics of DC-MQD lasers. The device characteristics in DC-MQD lasers were discussed in comparison with those in Uni-MQD lasers. Theoretical model regarding to DC-MQD gain media is then constructed to simulate our experimental observation in Section 3. Section 4 summarizes and concludes this paper.

2. Experimental Results

The active region of investigated laser structure was grown with DC-MQD stacks. It consisted of 10 layers of InAs QD which were capped by strain-reducing $In_{0.15}Ga_{0.85}As$ QW of varying thickness and spaced by GaAs of 33 nm. Three chirped wavelengths of long, medium, and short range with stacking numbers of two, three, and five layers (addressed as $2 \cdot QD_1$, $3 \cdot QD_2$ and $5 \cdot QD_3$) were designed with InGaAs QW thickness of 4, 3, and 1 nm, respectively. The schematic active region is shown in the inset of Figure 1b. Device fabrication of ridge waveguide lasers was outsourced to Union Optronics Corporation. As-cleaved laser bars were left unpacked for probe characterization under continuous-wave (CW) injection current at room temperature. The waveguide width and cavity length of investigated devices were 10 μm and 2.5 mm, respectively. The detailed crystal growth [8] and device fabrication [10] can be found in our previous publications.
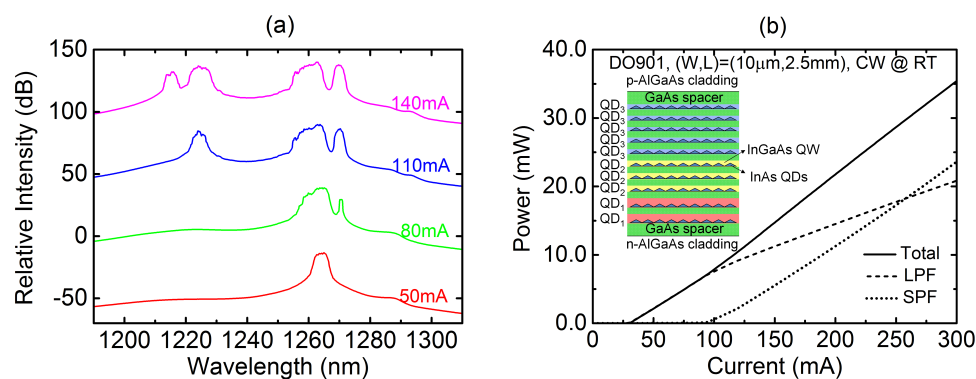

Figure 1. (**a**) the evolution of lasing spectra with injection current; (**b**) light-current (L-I) curves with optical long-pass filter (LPF), short-pass filter (SPF), and without optical filter.

Figure 1a shows the evolution of lasing spectra with injection current. The optical intensities are relative in decibel scale and shifted in vertical axis for clarity. At CW current of 50 mA, the first lasing peak emerges around 1265 nm. The spectral width broadens at 80 mA and splits into two groups of longitudinal modes. Note that longitudinal modes of 2.5-mm-cavity are too close to be resolved in our measurement resolution of 0.5 nm. At 100 mA, the second lasing peak emerges around 1225 nm while the two group-modes associated with the first peak broaden further. The spectral width of the second peak broadens with current and also splits into two groups at 140 mA. The two lasing wavelengths separate as far as 40 nm, which is larger than the inhomogeneous broadening width but smaller than the separation between GS and excited-state (ES) wavelength peaks (about 80 nm). Referring to photoluminescence measurement in [9], the two lasing wavelengths are identified as

GS emissions from $2 \cdot QD_1$ and $3 \cdot QD_2$, which are respectively addressed as GS1 and GS2 thereafter. To separate light intensities associated with GS1 and GS2 emissions, high performance (Optical Density ≥ 4.0) long-pass filter (LPF, Stock #89-659, Edmund Optics Inc., Barrington, NJ, USA) or short-pass filter (SPF, Stock #89-671) with sharp cut-off at 1250 nm is inserted before light detection. Figure 1b shows the light–current ($L - I$) characteristics with LPF, SPF, and without optical filter. The threshold currents associated with GS1 and GS2 emissions are 32 mA and 95 mA, respectively. The ratio of GS2 to GS1 threshold is less than 3. Moreover, it is anomalous to observe that GS1 lasing intensity neither saturates nor droops with increasing injection current upon the threshold of GS2 transitions.

For conventional 1.3-µm-range QD lasers with Uni-MQD active region, dual-wavelength lasing emissions were originated from GS and ES transitions which separated as far as 70–80 nm [11,12]. Moreover, the ratio of ES to GS threshold current was over 10 or 20 for uniformly stacked 3- or 5-layer QD lasers [11,12], respectively. For a 3-layer Uni-MQD laser under pulsed operation and above the ES threshold current, the $L - I$ curves of GS transition exhibited saturation for 2-mm-cavity device but dropped down to zero for 1.65-mm-cavity device [11]. In fact, saturation or depression of GS transitions after the threshold of ES transitions were also observed at high heatsink temperature and/or under CW operation [12,13]. The comprehensive numerical model was developed to explain the observation for Uni-MQD lasers [14] mentioned above. Investigation revealed incomplete gain clamping of ES population upon GS threshold. Actually, ES transitions intercept extra injection carriers upon ES threshold in Uni-MQD lasers.

Application of dual-wavelength lasers with Uni-MQD structure may be limited because the ES wavelength is far away from the GS wavelength and can be tuned only by growth condition; moreover, the GS emission intensities upon the ES threshold are saturated or dropped down to zero with increasing injection current. For dual-wavelength lasers with DC-MQD structure, the second lasing wavelength is also GS emissions and can be tailored easily by capping layer thickness. In addition, it is revealed for the first time that wavelength-resolved L-I characteristics exhibit non-saturated and linear relationship for both wavelengths. Dual-wavelength lasers with DC-MQD structure can surely benefit from the unusual characteristics in applications. To exploit the advantages of DC-MQD structure for further device optimization, it is imperative that a theoretical model is constructed for our dual-wavelength DC-MQD lasers.

3. Theoretical Simulations

The theoretical model consists of a system of coupled rate equations that describe temporal evolution of carrier populations among energy states as well as their interaction with optical photons. Charged carriers of electrons and holes, populated in respective energy states and recombined in pairs, are treated as excitons. Three types of excitonic energy states are considered in QDs, i.e., QW state, excited state (ES) and ground state (GS). The InGaAs QW is a common reservoir for carrier relaxation to ES where transitions between ES and ES occur only in the same QDs.

The rate equations for digitally chirped QD layers are modified from those for uniformly stacked multilayer QDs [15,16]. Table 1 lists all device parameters used in the present simulation. Note that three chirped wavelengths were designed in the experiment but only two are modeled in the simulation for computational efficiency. The third wavelength did not lase because its steady-state GS carrier population is low and population inversion cannot be achieved in the measurement range. The inhomogeneous broadening of a QD ensemble is described by Gaussian distribution function [16] and discretized with an energy resolution (ΔE) of 1 meV. The probability density functions for the *j*-th QD group of first and second chirped wavelengths are given by:

$$
\begin{aligned}
G_{1j} &= \frac{1}{\sqrt{2\pi}\sigma} exp\left(-\frac{E_j - E_1}{2\sigma^2}\right) \Delta E, \\
G_{2j} &= \frac{1}{\sqrt{2\pi}\sigma} exp\left(-\frac{E_j - E_2}{2\sigma^2}\right) \Delta E,
\end{aligned}
\tag{1}
$$

where E_1 and E_2 are the mean energies as well as the lasing peaks of longer- and medium-wavelength QD stacks, respectively. The standard deviation (σ) is related to the inhomogeneous broadening factor (Γ_{inh}) or the full-width-of-half-maximum (FWHM) of Gaussian distribution by $\Gamma_{inh} = (\sqrt{8\ln 2})\sigma$. The maximum numbers of GS and ES states for the *j*-th QD group, including stacking layer numbers (2 or 3), spin and energy degeneracies (D_g and D_e), are given by:

$$
\begin{aligned}
M_{g_1,j} &= 2D_g \cdot N_s \cdot W \cdot L \cdot G_{1j}, \\
M_{e_1,j} &= 2D_e \cdot N_s \cdot W \cdot L \cdot G_{1j}, \\
M_{g_2,j} &= 3D_g \cdot N_s \cdot W \cdot L \cdot G_{2j}, \\
M_{e_2,j} &= 3D_e \cdot N_s \cdot W \cdot L \cdot G_{2j},
\end{aligned}
\tag{2}
$$

where N_s is surface dot density per layer, and W and L are ridge width and cavity length, respectively. The optical gain (both GS and ES) can be simplified by multiplying a linear gain coefficient (g_0) by the carrier in excess of the transparency carrier and dividing by the total volume (V_t) [17]. Since longitudinal mode separation is less than 0.1 meV for 2.5-mm-long cavity; without loss of generality, we consider only photonic energies which are discretized exactly the same as excitonic energies. The constitutional optical gain of *k*-th photon energy that originated from *j*-th QD group of GS1 and GS2 is given by:

$$
\begin{aligned}
g_{kj}^{GS1} &= \frac{g_0}{V_t}\left(N_{g_1,j} - \frac{M_{g_1 j}}{2}\right) L(E_j, E_k), \\
g_{kj}^{GS2} &= \frac{g_0}{V_t}\left(N_{g_2,j} - \frac{M_{g_2,j}}{2}\right) L(E_j, E_k).
\end{aligned}
\tag{3}
$$

Table 1. Device parameters for digitally chirped multilayer quantum-dot (DC-MQD) lasers.

Symbol	Description	Value	Reference
ΔE	energy resolution	1 meV	
E_1, E_2	lasing energy peaks	0.98, 1.016 eV	
D_g, D_e	GS, ES degeneracy (with spin)	2, 4	[17]
N_s	QD surface density	4×10^{10} cm^{-2}	
W, L	waveguide width, cavity length	10, 2500 μm	
g_0	differential gain coefficient	10^{-15} cm^2	
V_t	total QD volume	10^{-9} cm^3	
Γ_{inh}	inhomgeneous broadening factor	30 meV	
Γ_{hom}	homogeneous broadening factor	13 meV	
n_r	refraction index	3.47	
β	spontaneous emission factor	10^{-5}	[14]
Γ_{a1}, Γ_{a2}	optical confinement factor	0.023, 0.047	
τ_p	photon lifetime	15 ps	
$\tau_{we_1}, \tau_{e_1 w}$	QW $\leftrightarrow$ ES1 transition time	2, 10 ps	[17]
$\tau_{we_2}, \tau_{e_2 w}$	QW $\leftrightarrow$ ES2 transition time	3, 10 ps	
$\tau_{e_1 g_1}, \tau_{g_1 e_1}$	ES1 $\leftrightarrow$ GS1 transition time	8, 18 ps	[17]
$\tau_{e_2 g_2}, \tau_{g_2 e_2}$	ES2 $\leftrightarrow$ GS2 transition time	8, 18 ps	
τ_w	QW spontaneous lifetime	5000 ps	[17]
τ_{e_1}, τ_{g_1}	ES1, GS1 spontaneous lifetime	500, 2000 ps	[17]
τ_{e_2}, τ_{g_2}	ES2, GS2 spontaneous lifetime	200, 1000 ps	

The optical gain is homogeneously broadened by a Lorentz distribution function [16] given as

$$
L(E_j, E_k) = \frac{1}{\pi} \frac{(\Gamma_{hom}/2)}{(E_j - E_k)^2 + (\Gamma_{hom}/2)^2},
\tag{4}
$$

where the homogeneous broadening factor (Γ_{hom}) is its FWHM. The spontaneous emitted photons associated with ES1 and ES2 are not considered in gain calculation because they are well below respective transparent population in our investigated range of injection current.

The excitons (electron-hole pairs) in the QW, ES1, GS1, ES2 and GS2 states of *j*-th QD group (N_w, $N_{e_1,j}$, $N_{g_1,j}$, $N_{e_2,j}$ and $N_{g_2,j}$, respectively) as well as *k*-th spectral photon energy originated from GS1 and GS2 ($S_{1,k}$ and $S_{2,k}$, respectively) in DC-MQD lasers are coupled by the following system of nonlinear differential equations:

$$\frac{dN_w}{dt} = \frac{I}{e} + \sum_j \left\{ \frac{N_{e_1,j}}{\tau_{e_1w}} - \frac{N_w}{\tau_{we_1}} G_{1j} \left(1 - \frac{N_{e_1,j}}{M_{e_1,j}}\right) + \frac{N_{e_2,j}}{\tau_{e_2w}} - \frac{N_w}{\tau_{we_2}} G_{2j} \left(1 - \frac{N_{e_2,j}}{M_{e_2,j}}\right) \right\} - \frac{N_w}{\tau_w}, \tag{5}$$

$$\frac{dN_{e_1,j}}{dt} = \frac{N_w}{\tau_{we_1}} G_{1j} \left(1 - \frac{N_{e_1,j}}{M_{e_1,j}}\right) - \frac{N_{e_1,j}}{\tau_{e_1w}} + \frac{N_{g_1,j}}{\tau_{g_1e_1}} \left(1 - \frac{N_{e_1,j}}{M_{e_1,j}}\right) - \frac{N_{e_1,j}}{\tau_{e_1g_1}} \left(1 - \frac{N_{g_1,j}}{M_{g_1,j}}\right) - \frac{N_{e_1,j}}{\tau_{e_1}}, \tag{6}$$

$$\frac{dN_{g_1,j}}{dt} = \frac{N_{e_1,j}}{\tau_{e_1g_1}} \left(1 - \frac{N_{g_1,j}}{M_{g_1,j}}\right) - \frac{N_{g_1,j}}{\tau_{g_1e_1}} \left(1 - \frac{N_{e_1,j}}{M_{e_1,j}}\right) - \frac{C_0\Gamma_{a1}}{n_r} \sum_k g_{kj}^{GS1} (S_{1,k} + S_{2,k}) - \frac{N_{g_1,j}}{\tau_{g_1}}, \tag{7}$$

$$\frac{dS_{1,k}}{dt} = \frac{C_0\Gamma_{a1}}{n_r} \sum_j g_{kj}^{GS1} S_{1,k} - \frac{S_{1,k}}{\tau_p} + \beta \frac{N_{g_1,k}}{\tau_{g_1}}, \tag{8}$$

$$\frac{dN_{e_2,j}}{dt} = \frac{N_w}{\tau_{we_2}} G_{2j} \left(1 - \frac{N_{e_2,j}}{M_{e_2,j}}\right) - \frac{N_{e_2,j}}{\tau_{e_2w}} + \frac{N_{g_2,j}}{\tau_{g_2e_2}} \left(1 - \frac{N_{e_2,j}}{M_{e_2,j}}\right) - \frac{N_{e_2,j}}{\tau_{e_2g_2}} \left(1 - \frac{N_{g_2,j}}{M_{g_2,j}}\right) - \frac{N_{e_2,j}}{\tau_{e_2}}, \tag{9}$$

$$\frac{dN_{g_2,j}}{dt} = \frac{N_{e_2,j}}{\tau_{e_2g_2,j}} \left(1 - \frac{N_{g_2,j}}{M_{g_2,j}}\right) - \frac{N_{g_2,j}}{\tau_{g_2e_2}} \left(1 - \frac{N_{e_2,j}}{M_{e_2,j}}\right) - \frac{C_0\Gamma_{a2}}{n_r} \sum_k g_{kj}^{GS2} (S_{1,k} + S_{2,k}) - \frac{N_{g_2,j}}{\tau_{g_2}}, \tag{10}$$

$$\frac{dS_{2,k}}{dt} = \frac{C_0\Gamma_{a2}}{n_r} \sum_j g_{kj}^{GS2} S_{2,k} - \frac{S_{2,k}}{\tau_p} + \beta \frac{N_{g_2,k}}{\tau_{g_2}}, \tag{11}$$

where I is pumping current, e is elementary charge, C_0 is vacuum speed of light, n_r is refractive index, β is spontaneous emission factor, Γ_{a1} and Γ_{a2} are optical confinement factors for $2 \cdot QD_1$ and $3 \cdot QD_2$ stacks, respectively. The photon lifetime (τ_p) is determined by the internal and mirror losses of about 7.7 cm^{-1}. The spontaneous lifetime for each energy state and transition time between adjacent energy states are also defined in Table 1. The time constants associated with GS1/ES1 states are referenced from [17], while those associated with GS2/ES2 states are obtained by fitting the second threshold current. Note that the carrier and photon rate equations associated with the second chirped wavelength are treated independently in Equations (9)–(11). More chirped wavelengths can be included accordingly. In addition, nonlinear coupling between photons and carriers in Equations (7) and (10) deals with total spectral photons ($S_{1,k} + S_{2,k}$). In comparison to these equations with individual spectral photons, the calculated light intensities are overestimated.

Figure 2a shows simulated photon number spectra ($S_{1,k} + S_{2,k}$) at four injection currents. The photon numbers are also scaled in logarithmic scale and shifted in vertical axis. The flattened lasing peaks are due to insufficient photon spectral resolution ($\Delta E = 1$ meV) in the simulation. The spectra integrated photon number versus injection current for GS1, GS2 and total emitted photons are shown in Figure 2b. After the threshold of GS2 transitions, neither saturation nor depression is observed for GS1 lasing emissions. This is because GS2 transitions do not intercept but compete for extra injection carriers in the common reservoir. The simulations in Figure 2 qualitatively reproduce very well the experiments in Figure 1.
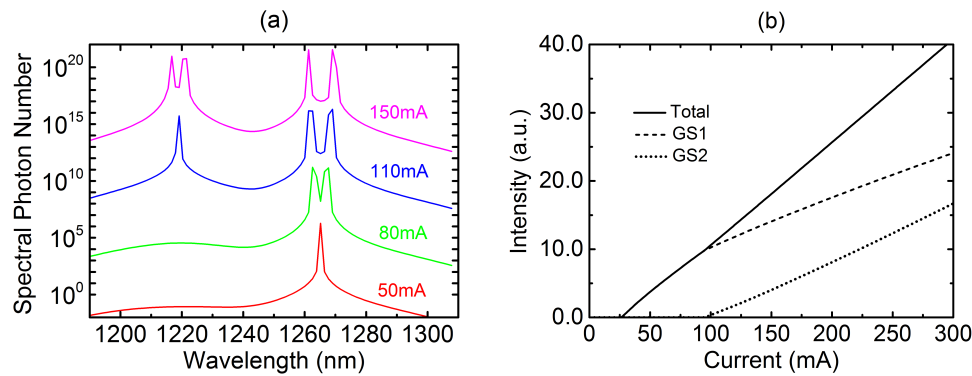
Figure 2. Simulation of digitally chirped multilayer quantum-dot (DC-MQD) lasers: (**a**) L-I characteristics and (**b**) lasing spectra.

The spectral widths of GS1 and GS2 lasing emissions broaden with increasing current. In addition, the near-threshold single peak splits into two increasingly separated peaks (or two groups of longitudinal modes) at well above the threshold. The similar spectral broadening and splitting were also measured and simulated in Uni-MQD lasers [18]. The spectral splitting of group modes is associated with spectral hole-burning, which leads to a slightly reduced optical gain at excitonic peaks. Figure 3 shows the carrier population versus injection current at excitonic peaks of GS1, GS2, ES1 and ES2 transitions. The carrier population at the excitonic peak (E_1 or E_2) is pinned but somewhat depressed above the threshold. The carriers are somewhat depleted by abundant lasing photons as can be seen in Equations (7) or (10). Moreover, the optical gain on both sides of the excitonic peak are slightly enhanced to achieve the threshold because of an increasing carrier population as well as a lower transparency carrier number. Since QD size distribution and carrier population in the experiment are not ideally symmetric, asymmetric spectral splitting results in Figure 1a.
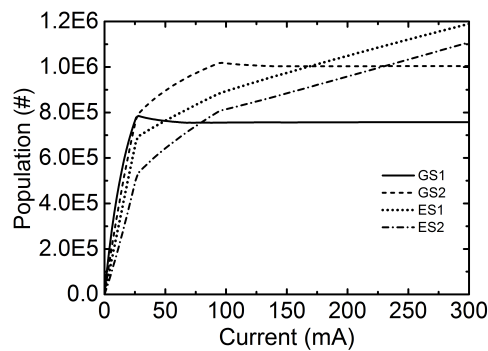

Figure 3. Carrier population versus injection current at excitonic peaks of GS1, GS2, ES1, and ES2 transitions.

4. Conclusions

We have studied the dual-wavelength lasing emissions of digitally chirped multilayer QD lasers by their light-current characteristics and lasing spectra. The two lasing wavelengths are both ascribed to GS emissions but originated from two stacks of QD multilayers. They are wavelength resolved by optical filters in the experiment and separately treated in the simulation. The first GS lasing intensity upon the threshold of second GS transitions still increases with increasing current but with slightly reduced slope efficiency. The lasing spectra broadens with increasing injection because of inhomogeneous broadening and splits into group of modes at high injection because of spectral hole-burning. The simulated results reproduce the experimental measurements very well. With the rate–equation model developed in this paper, we can engineer and optimize novel devices incorporating digitally chirped multilayer QD active region.

References

1. Kirstaedter, N.; Ledentsov, N.N.; Grundmann, M.; Bimberg, D.; Ustinov, V.M.; Ruvimov, S.S.; Maximov, M.V.; Kop'ev, P.S.; Alferov, Z.I.; Richter, U.; et al. Low threshold, large To injection laser emission from (InGa)As quantum dots. *Electron. Lett.* **1994**, *30*, 1416–1417. [CrossRef]

2. Schmidt, O.G.; Kirstaedter, N.; Ledentsov, N.N.; Mao, M.H.; Bimberg, D.; Ustinov, V.M.; Egorov, A.Y.; Zhukov, A.E.; Maximov, M.V.; Kop'ev, P.S.; et al. Prevention of gain saturation by multu-layer quantum dot lasers. *Electron. Lett.* **1996**, *32*, 1302–1304. [CrossRef]

3. Saito, H.; Nishi, K.; Ogura, I.; Sugou, S.; Sugimoto, Y. Room-temperature lasing operation of a quantum-dot vertical-cavity surface-emitting laser. *Appl. Phys. Lett.* **1996**, *69*, 3140–3142. [CrossRef]

4. Li, L.H.; Rossetti, M.; Fiore, A.; Occhi, L.; Velez, C. Wide emission spectrum from superluminescent diodes with chirped quantum dot multilayers. *Electron. Lett.* **2005**, *41*, 41–43. [CrossRef]

5. Djie, H.S.; Ooi, B.S.; Fang, X.M.; Wu, Y.; Fastenau, J.M.; Liu, W.K.; Hopkinson, M. Room-temperature broadband emission of an InGaAs/GaAs quantum dots laser. *Opt. Lett.* **2007**, *32*, 44–46. [CrossRef] [PubMed]

6. Li, L.H.; Rossetti, M.; Fiore, A. Chirped multiple InAs quantum dot structure for wide spectrum device applications. *J. Cryst. Growth* **2005**, *278*, 680–684. [CrossRef]

7. Lin, G.; Lin, K.F.; Lai, C.M. Multiwavelength Quantum Dot Laser Element. U.S. Patent No. 7,573,926, 11 August 2009.

8. Lin, G.; Chang, C.Y.; Tseng, W.C.; Lee, C.P.; Lin, K.F.; Xuan, R.; Chi, J.Y. Novel chirped multilayer quantum-dot lasers. In Proceedings of the Semiconductor Lasers and Laser Dynamics III, Strasbourg, France, 7–9 April 2008; Volume 6997, p. 69970R.

9. Lin, G.; Su, P.Y.; Cheng, H.C. Low threshold current and widely tunable external cavity lasers with chirped multilayer InAs/InGaAs/GaAs quantum-dot structure. *Opt. Express* **2012**, *20*, 3941–3947. [CrossRef] [PubMed]

10. Chen, Y.C.; Hsien, P.H.; Lin, G. Chirped multilayer quantum-dot mode-locked lasers with dualwavelength and ground-state lasing emissions. *J. Nanophotonics* **2019**, *13*, 016001.

11. Markus, A.; Chen, J.X.; Paranthoën, C.; Fiore, A.; Platz, C.; Gauthier-Lafaye, O. Simultaneous two-state lasing in quantum-dot lasers. *Appl. Phys. Lett.* **2003**, *82*, 1818–1820. [CrossRef]

12. Zhukov, A.E.; Kovsh, A.R.; Livshits, D.A.; Ustinov, V.M.; Alferov, Z.I. Ouput power and its limitation in ridge-waveguide 1.3 μm wavelength quantum-dot lasers. *Semicond. Sci. Technol.* **2003**, *18*, 774–781. [CrossRef]

13. Lin, G.; Wang, J.S.; Hsiao, R.S.; Wei, L.; Wu, Y.T.; Chi, J.Y.; Kovsh, A.R.; Livshits, D.A. The spectral and temperature behavior of single mode InAs/InGaAs/GaAs quantum dot lasers lasing at 1.3 μm range. In Proceedings of the Digest of 30th International Electron Devices and Materials Symposia, Taipei, Taiwan, 20–21 December 2002; p. 12.1.

14. Markus, A.; Chen, J.X.; Gauthier-Lafaye, O.; Provost, J.G.; Paranthoën, C.; Fiore, A. Impact of intraband relaxation on the performance of a quantum-dot laser. *IEEE J. Sel. Top. Quantum Electron.* **2003**, *9*, 1308–1314. [CrossRef]

15. Meuer, C.; Kim, J.; Laemmlin, M.; Liebich, S.; Capua, A.; Eisenstein, G.; Kovsh, A.R.; Mikhrin, S.S.; Krestnikov, I.L.; Bimberg, D. Static gain saturation in quantum dot semiconductor optical amplifiers. *Opt. Express* **2008**, *16*, 8269–8279. [CrossRef] [PubMed]

16. Sugawara, M.; Mukai, K.; Nakata, Y.; Ishikawa, H. Effect of homogeneous broadening of optical gain on lasing spectra in self-assembled In$_x$Ga$_{1-x}$As/GaAs quantum dot lasers. *Phys. Rev. B* **2000**, *61*, 7595–7603. [CrossRef]

17. Cataluna, M.A.; Nikitchev, D.I.; Mikroulis, S.; Simos, H.; Simos, C.; Mesaritakis, C.; Syvridis, D.; Krestnikov, I.; Livshits, D.; Rafailov, E.U. Dual-wavelength mode-locked quantum-dot laser, via ground and excited state transitions: Experimental and theoretical investigation. *Opt. Express* **2010**, *18*, 12832–12838. [CrossRef] [PubMed]

18. Sugawara, M.; Hatori, N.; Ebe, H.; Ishida, M.; Arakawa, Y.; Akiyama, T.; Otsubo, K.; Nakata, Y. Modeling room-temperature lasing spectra of 1.3-μm self-assembled InAs/GaAs quantum-dot lasers: Homogeneous broadening of optical gain under current injection. *J. Appl. Phys.* **2005**, *97*, 043523. [CrossRef]